Journal of Solid Mechanics Vol. 5, No. 2 (2013) pp. 161-173

Frequency Analysis of FG Sandwich Rectangular Plates with a Four-Parameter Power-Law Distribution

S. Kamarian[1], M.H. Yas[2,*], A. Pourasghar[3]

[1]*Young Researchers and Elite Club, Kermanshah Branch, Islamic Azad University, Kermanshah, Iran*
[2]*Department of Mechanical Engineering, Razi University, Kermanshah, Iran*
[3]*Young Researchers and Elite Club, Central Tehran Branch, Islamic Azad University, Tehran, Iran*

Received 21 March 2013; accepted 12 May 2013

ABSTRACT

An accurate solution procedure based on the three-dimensional elasticity theory for the free vibration analysis of Functionally Graded Sandwich (FGS) plates is presented. Since no assumptions on stresses and displacements have been employed, it can be applied to the free vibration analysis of plates with arbitrary thickness. The two-constituent FGS plate consists of ceramic and metal graded through the thickness, from one surface of the each sheet to the other according to a generalized power-law distribution with four parameters. The benefit of using generalized power-law distribution is to illustrate and present useful results arising from symmetric, asymmetric and classic profiles. Using the Generalized Differential Quadrature (GDQ) method through the thickness of the plate, further allows one to deal with FG plates with an arbitrary thickness distribution of material properties. The fast rate of convergence and accuracy of the method are investigated through the different solved examples. The effects of different geometrical parameters such as the thickness-to-length ratio, different profiles of materials volume fraction and four parameters of power-law distribution on the vibration characteristics of the FGS plates are investigated. Interesting result shows that by utilizing a suitable four-parameter model for materials volume fraction, frequency parameter can be obtained more than the frequency parameter of the similar FGS plate with sheets made of 100% ceramic and at the same time lighter. Also, results show that frequencies of symmetric and classic profiles are smaller and larger than that of other types of FGS plates respectively. The solution can be used as benchmark for other numerical methods and also the refined plate theories.

Keywords: Elasticity solution; Sandwich plate; Functionally graded materials; Generalized power-law distribution; GDQ method

1 INTRODUCTION

SANDWICH structures are used in a variety of engineering applications including aircraft, construction and transportation where strong, stiff and light structures are required. The advantages of these structures are that it provides high specific stiffness and strength for a low-weight consideration. Due to the mismatch of stiffness properties between the face sheets and the core, sandwich plates are susceptible to face sheet/core debonding, which is a major problem in sandwich construction, especially under impact loading. To increase the resistance of sandwich plates to this type of failure, the concept of a Functionally Graded Material (FGM) is being actively explored in sandwich structure design. FGMs are achieved by gradually changing the composition of the constituent

* Corresponding author. Tel.: +98 831 427 4538 ; Fax: +98 831 427 4542.
E-mail address: yas@razi.ac.ir (M.H. Yas).

materials along one (or more) direction(s), usually in the thickness direction, to obtain smooth variation of material properties and optimum response to externally applied loading. Various material profiles through the functionally graded plate thickness can be illustrated by using a generalization of the power-law distribution. Recently, some researchers have studied free vibrations of four-parameter functionally graded structures [1, 4].

A lot of number of plates with different shapes, size, and thickness variations and boundary conditions has been the subject of numerous investigations and those play an important role in aerospace, marine, civil, mechanical, electronic and nuclear engineering problems. Malekzadeh [5] studied three-dimensional free vibrations analyses of thick functionally graded plates on elastic foundations by using Differential Quadratic (DQ) method. Yas and Sobhani analyzed free vibration of continuous grading fiber reinforced plates on elastic foundation [6]. Matsunaga analyzed free vibration and stability of functionally graded plates according to a 2D higher-order deformation theory [7].

Though there are research works reported on general sandwich structures, a few works have been done to consider the vibration behavior of FGM sandwich (FGS) structures. Li et al. [8] studied free vibrations of FGS rectangular plates with simply supported and clamped edges. Zenkour [9, 10] presented a two dimensional solution to study the bending, buckling and free vibration of simply supported FG ceramic–metal sandwich plates. Khalili and Mohammadi analyzed the free vibration of a rectangular sandwich plate with functionally graded face sheets [11]. The material properties of FG face sheets were assumed to be temperature-dependent by a third-order function of temperature and vary continuously through the thickness according to a power-law distribution in terms of the volume fractions of the constituents. The results showed that as the side-to-thickness ratio, the core-to-face sheet thickness ratio and the temperature are changed, a significant effect on the fundamental frequency parameter is observed. Natarajan and Manickam investigated bending and vibration of functionally graded material sandwich plates using QUAD-8 shear flexible element developed based on higher order structural theory [12].They considered two types of sandwich FGM plates, viz., homogeneous face sheets with FGM core and FGM face sheets with homogeneous hard core. The influence of the gradient index and the plate aspect ratio on the response of different sandwich FGM plates was examined in their work. Static, free vibration and buckling of isotropic and sandwich functionally graded plates was analyzed by Neves et al. [13]. They utilized a quasi-3D higher-order shear deformation theory and a meshless technique for their investigations. Sobhy analyzed vibration and buckling behavior of Exponentially Graded Material (EGM) sandwich plate resting on Pasternak foundation under various boundary conditions [14].The influences of the geometrical parameters, inhomogeneity parameter and the foundation parameters on the natural frequencies and critical buckling loads were investigated in their work. Recently Xiang et al. [15] analyzed the free vibration of sandwich plate with functionally graded face and homogeneous core using meshless global collocation method on the thin plate spline radial basis function and nth-order shear deformation theory.

The present research is in the continuation of previous works on four-parameters FGM structures [2-4]. In order to distinguish the present work from the above pertinent literature, first, the accuracy of the three-dimensional elasticity theory is discussed. Then, effect of functionally graded face sheets on free vibration of simply supported sandwich rectangular plates is investigated. The fiber-reinforced composite material studied in the present work consists of alumina (ceramic) fibers embedded in aluminum (metal) matrix with the fiber volume fraction graded according to a four-parameter power-law distribution through thickness. Frequency parameters are obtained by using numerical technique termed the GDQM which leads to a generalized eigen value problem. GDQ is found to be a simple and efficient numerical technique for solving partial differential equations as reported by Bellman et al. [16]. The mathematical fundamental and recent development of GDQ method as well as its' major applications in engineering were discussed in detail in Ref. [17].

2 PROBLEM DESCRIPTION

2.1 FGM material properties

Consider a thick FGS plate as shown in Fig. 1. A Cartesian coordinate system (x, y, z) is used to label the material point of the plate in the unstressed reference configuration.

The plate has continuous grading of fiber reinforcement through thickness. h, h_c, and h_f are the thickness of plate, core and face sheets respectively and the plate is assumed to be symmetric with respect to its mid-plane $z = 0$. The Young's modulus $E(z)$, Poisson's ratio $\nu(z)$ and mass density $\rho(z)$ of the FGS plate can be expressed as [1]:

$$E(z) = (E_c - E_m)V_c \quad , \quad \rho(z) = (\rho_c - \rho_m)V_c \quad , \quad \nu(z) = (\nu_c - \nu_m)V_c \tag{1}$$

where indexes *m* and *c* present metal and ceramic material respectively. In the present work, by idealizing Ref. [1], the metal volume fraction of FGS plate is assumed as follows:

$$V_m(z)=\begin{cases}\left[1-a(1-\dfrac{z+h/2}{h_f})+b(1-\dfrac{z+h/2}{h_f})^c\right]^p, & -\dfrac{h}{2}\le z\le -\dfrac{h}{2}+h_f\\ 1, & -\dfrac{h}{2}+h_f\le z\le \dfrac{h}{2}+h_f\\ \left[1-a(1+\dfrac{z-h/2}{h_f})+b(1+\dfrac{z-h/2}{h_f})^c\right]^p, & \dfrac{h}{2}-h_f\le z\le \dfrac{h}{2}\end{cases}\quad , \quad V_c=1-V_m \tag{2}$$

where the power-law index p $(0\le p\le\infty)$ and the parameters *a, b, c* dictate the metal variation profile through the FGS plate thickness. It should be noticed that the values of parameters *a, b* and *c* must be chosen so that $0\le V_m\le 1$. According to the relation (2), the core of FGS plate and the inner surfaces of the sheets are metal rich, where as the outer surfaces of the sheets can be metal rich, ceramic rich or made of a mixture of the two constituents. The through-thickness variations of Young's modulus of FGS plate for some profiles are illustrated in Fig. 2. The relevant material properties for the constituent materials considered in this work are as follows [15]:

$$E_c=380\ \ \text{Gpa}\ ,\ \rho_c=3800\ \ kg/m^3\ ,\ \upsilon_c=0.3\ \ ,\ \ E_m=70\ \ \text{Gpa}\ ,\ \upsilon_m=0.3\ ,\ \rho_m=2707\ \ kg/m^3$$

In Fig. 2a the classical Young's modulus profiles are presented as special cases of the general distribution laws (2) by setting *a=1, b=0* which has been recently considered for analysis of a FGS rectangular plate by Xiang et al. [15]. In Figs. 2b and 2c, by setting *a=1, b=1, c=2* and *a=1, b*=1, *c=4* symmetric and asymmetric profiles respect to the mid-planes of the sheets are obtained respectively. In Fig. 2e, Young's modulus profiles for the different values of parameter *c* is shown by considering *p*=1 in which Young's modulus profile along *z* direction becomes asymmetric with increasing parameter *c*. Young's modulus on the inner and outer surfaces of sheets for the different values of parameter *c* is the same in Fig. 2e.

2.2 The basic formulation

The mechanical constitutive relations which relates the stresses to the strains are as [6]:

$$\begin{Bmatrix}\sigma_x\\ \sigma_y\\ \sigma_z\\ \tau_{zy}\\ \tau_{xz}\\ \tau_{xy}\end{Bmatrix}=\begin{bmatrix}C_{11} & C_{12} & C_{13} & 0 & 0 & 0\\ C_{12} & C_{22} & C_{23} & 0 & 0 & 0\\ C_{13} & C_{23} & C_{33} & 0 & 0 & 0\\ 0 & 0 & 0 & C_{44} & 0 & 0\\ 0 & 0 & 0 & 0 & C_{55} & 0\\ 0 & 0 & 0 & 0 & 0 & C_{66}\end{bmatrix}\begin{Bmatrix}\varepsilon_x\\ \varepsilon_y\\ \varepsilon_z\\ \gamma_{zy}\\ \gamma_{xz}\\ \gamma_{xy}\end{Bmatrix} \tag{3}$$

In the absence of body forces, the governing equations are as follows [6]:

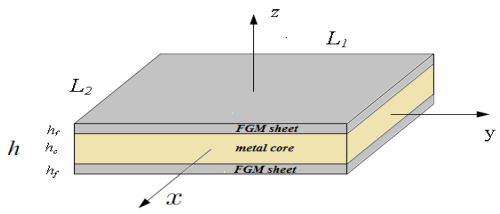

Fig. 1
Geometry of the FGS rectangular plate.

$$\begin{aligned}
&\frac{\partial \sigma_x}{\partial x}+\frac{\partial \tau_{xy}}{\partial y}+\frac{\partial \tau_{xz}}{\partial z}=\rho\frac{\partial^2 u}{\partial t^2}\\
&\frac{\partial \tau_{xy}}{\partial x}+\frac{\partial \sigma_y}{\partial y}+\frac{\partial \tau_{yz}}{\partial z}=\rho\frac{\partial^2 v}{\partial t^2}\\
&\frac{\partial \tau_{xz}}{\partial x}+\frac{\partial \tau_{yz}}{\partial y}+\frac{\partial \sigma_z}{\partial z}=\rho\frac{\partial^2 w}{\partial t^2}
\end{aligned} \tag{4}$$

Strain- displacement relations are expressed as [6]:

$$\begin{aligned}
&\varepsilon_z=\frac{\partial w}{\partial z},\varepsilon_y=\frac{\partial v}{\partial y},\varepsilon_x=\frac{\partial u}{\partial x},\gamma_{xy}=\frac{\partial v}{\partial x}+\frac{\partial u}{\partial y}\\
&\gamma_{xz}=\frac{\partial w}{\partial x}+\frac{\partial u}{\partial z},\gamma_{yz}=\frac{\partial v}{\partial z}+\frac{\partial w}{\partial y}
\end{aligned} \tag{5}$$

where u, v, w are displacement components along the *x, y* and *z* axes respectively. Upon substitution Eq. (5) into (3) and then into (4), the following equations of motion as matrix form are obtained in term of displacement components [6]:

$$\begin{bmatrix} L_{1x} & L_{1y} & L_{1z}\\ L_{2x} & L_{2y} & L_{2z}\\ L_{3x} & L_{3y} & L_{3z}\end{bmatrix}\begin{Bmatrix} u\\ v\\ w\end{Bmatrix}=\begin{Bmatrix} \rho\ddot{u}\\ \rho\ddot{v}\\ \rho\ddot{w}\end{Bmatrix} \tag{6}$$

where coefficients L_{ij} are given in Appendix A. For a simply supported rectangular plate, the boundary conditions can be expressed on the x-constant as well as y-constant edges as [6]:

$$u_{,x}=v=w=0 \qquad ,u=v_{,y}=w=0 \tag{7}$$

Moreover, for the lower and upper surfaces of the plate, it can be written:

$$\sigma_z=\tau_{zx}=\tau_{zy}=0 \quad at \quad z=\frac{h}{2},\ z=-\frac{h}{2} \tag{8}$$

Using the method of separation of variables, it is possible to seek solutions that are harmonic in time and their frequency is ω. The displacements can be written as follows [6]:

$$\begin{aligned}
&u=\sum_{m=1}^{\infty}\sum_{n=1}^{\infty}U(z)\cos(\beta_m x)\sin(P_n y)e^{iwt}\\
&v=\sum_{m=1}^{\infty}\sum_{n=1}^{\infty}V(z)\sin(\beta_m x)\cos(P_n y)e^{iwt}\\
&w=\sum_{m=1}^{\infty}\sum_{n=1}^{\infty}W(z)\sin(\beta_m x)\sin(P_n y)e^{iwt}
\end{aligned} \tag{9}$$

where $\beta_m=\frac{m\pi}{L_2}(m=1,2,...)$ and $p_n=\frac{n\pi}{L_1}(n=1,2,...)$, *m* and *n* are wave numbers along *x* and *y* directions respectively. Inserting these displacement components into the equations of motion (6), one obtains a set of coupled differential equations with variable coefficients [6].

$$
\begin{aligned}
&-C_{11}\beta_m{}^2U - C_{12}\beta_m p_n V + C_{13}\beta_m \frac{\partial W}{\partial z} - p_n{}^2 C_{66}U - C_{66}\beta_m p_n V + \frac{\partial C_{55}}{\partial z}\beta_m W + C_{55}\beta_m \frac{\partial W}{\partial z} + \frac{\partial C_{55}}{\partial z}\frac{\partial U}{\partial z} \\
&+C_{55}\frac{\partial^2 U}{\partial z^2} = -\rho\omega^2 U \\
&-C_{66}\beta_m p_n U - C_{66}\beta_m{}^2 V - C_{12}\beta_m p_n U - C_{22}p_n{}^2 V + C_{23}p_n \frac{\partial^2 W}{\partial z} + \frac{\partial C_{44}}{\partial z}\frac{\partial V}{\partial z} + C_{44}\frac{\partial^2 V}{\partial z^2} \\
&+\frac{\partial C_{44}}{\partial z}p_n W + C_{44}p_n \frac{\partial W}{\partial z} = -\rho\omega^2 V \\
&-C_{55}\beta_m{}^2 W - C_{55}\beta_m \frac{\partial U}{\partial z} - C_{44}p_n \frac{\partial V}{\partial z} - C_{44}p_n{}^2 W - \frac{\partial C_{13}}{\partial z}\beta_m U - C_{13}\beta_m \frac{\partial U}{\partial z} - \frac{\partial C_{23}}{\partial z}p_n V \\
&-C_{23}p_n \frac{\partial V}{\partial z} + \frac{\partial C_{33}}{\partial z}\frac{\partial W}{\partial z} + C_{33}\frac{\partial^2 W}{\partial z^2} = -\rho\omega^2 W
\end{aligned}
\tag{10}
$$

2.3 GDQ solution of governing equations

The GDQ approach is used to obtain the natural frequencies of FGS plate. This method approximates the spatial derivative of a function of given grid point as a weighted linear sum of all the functional value at all grid point in the whole domain. The computation of weighting coefficient by GDQ is based on an analysis of a high order polynomial approximation and the analysis of a linear vector space. The weighting coefficients of the first-order derivative are calculated by a simple algebraic formulation, and the weighting coefficient of the second-and higher-order derivatives are given by a recurrence relationship. In the purposed method, the nth order of a continuous function *f(x, z)* with respect to *x* at a given point x_i can be approximated as a linear sum of weighting values at all of the discrete point in the domain of *x* , i.e. [18]:

$$
\frac{\partial f^{n(x_i,z)}}{\partial x^n} = \sum_{k=1}^{N} c_{ik}^n f(x_{ik}, z), (i = 1, 2, N \quad n = 1, 2, ..., n-1)
\tag{11}
$$

where *N* is the number of sampling points, and $\boldsymbol{C}_{ij}^{n}$ is the x_i dependent weight coefficients.

In order to determine the weighting coefficients $\boldsymbol{C}_{ij}^{n}$, the Lagrange interpolation basic functions are used as test functions, and explicit formulation for computing these weighting coefficients can be obtained [18]:

$$
c_{i,j}^{(1)} = \frac{M^{(1)}(x_i)}{(x_i - x_j)M^{(1)}(x_i)} \quad , \quad i, j = 1, 2, ..., N \quad , \quad i \neq j
\tag{12}
$$

where

$$
M^{(1)}(x_i) = \prod_{j=1, i\neq j}^{N} (x_i - x_j)
\tag{13}
$$

For the first-order derivative; i.e. *n=1* and for higher-order derivative, one can use the following relations iteratively [18]:

$$
c_{i,j}^{n} = n\left(c_{i,j}^{(n-1)} c_{i,j}^{(1)} - \frac{c_{i,j}^{(n-1)}}{(x_i - x_j)} \right), \quad i, j = 1, 2, ..., N \ , \ i \neq j \ , \ n = 2, 3, n-1
\tag{14}
$$

$$
c_{i,j}^{(n)} = -\sum_{j=1, i\neq j}^{N} c_{i,j}^{(n)} \quad , \quad i = 1, 2, ..., N \quad , \quad n = 1, 2, ..., N-1
\tag{15}
$$

A simple and natural choice of the grid distribution is the uniform grid spacing rule. However, it was found that

non-uniform grid spacing yields results with better accuracy [19]. Hence, in this work, the Chebyshev-Gauss-Labatto quadrature points are used, that is [18],

$$x_i = \frac{1}{2}\left(1-\cos\left(\frac{i-1}{n-1}\pi\right)\right) \qquad i=1,2,...,N \tag{16}$$

More details about GDQ method can be found in Ref. [17].

By applying the GDQ method to Eq. (10), the following equations are obtained:

$$\begin{aligned}
&-\left(C_{11}\beta_m{}^2 + p_n{}^2 C_{66}\right)U_i - \left(C_{12}+C_{66}\right)\beta_m p_n V_i + \frac{\partial C_{55}}{\partial z}\beta_m W_i + \sum_{k=1}^{N}\left(\frac{\partial C_{55}}{\partial z}c_{ik}^{(1)} + C_{55}c_{ik}^{(2)}\right)U_k \\
&+\sum_{k=1}^{N}\left(C_{13}+C_{55}\right)\beta_m c_{ik}^{(1)} W_k = -\rho_i\omega^2 U_i \\
&-\left(C_{66}+C_{12}\right)\beta_m p_n U_i - \left(C_{66}\beta_m{}^2 + C_{22}p_n{}^2\right)V_i + \frac{\partial C_{44}}{\partial z}p_n W_i + \sum_{k=1}^{N}\left(\frac{\partial C_{44}}{\partial z}c_{ik}^{(1)} + C_{44}c_{ik}^{(2)}\right)V_k \\
&+\sum_{k=1}^{N}\left(C_{23}+C_{44}\right)p_n c_{ik}^{(1)} W_k = -\rho_i\omega^2 V_i \\
&-\frac{\partial C_{13}}{\partial z}\beta_m U_i - \frac{\partial C_{23}}{\partial z}p_n V_i - \left(C_{55}\beta_m{}^2 + C_{44}p_n{}^2\right)W_i - \left(C_{55}+C_{13}\right)\beta_m\sum_{k=1}^{N}c_{ik}^{(1)}U_k - \left(C_{44}+C_{23}\right)p_n\sum_{k=1}^{N}c_{ik}^{(1)}V_k \\
&+\sum_{k=1}^{N}\left(\frac{\partial C_{33}}{\partial z}c_{ik}^{(1)} + C_{33}c_{ik}^{(2)}\right)W_k = -\rho_i\omega^2 W_i
\end{aligned} \tag{17}$$

In the above equation $c_{ik}^{(1)}$ and $c_{ik}^{(2)}$ are the weighting coefficients of the first and second order derivatives. In a similar manner the boundary conditions can be discretized. For this purpose, using Eq.(8) and DQ discretization rule for special derivatives, the boundary conditions at *z=-h/2* and *z=h/2* become:

$$\begin{aligned}
&C_{55}c_{11}^{(1)}U_1 + C_{55}c_{1N}^{(1)}U_N + C_{55}\beta_m W_1 + C_{55}\sum_{k=2}^{N-1}c_{1k}^{(1)}U_k = 0 \\
&C_{44}c_{11}^{(1)}V_1 + C_{44}c_{1N}^{(1)}V_N + C_{44}p_n W_1 + C_{44}\sum_{k=2}^{N-2}c_{1k}^{(1)}V_k = 0 \\
&-C_{13}\beta_m U_1 - C_{23}p_n V_1 + C_{33}c_{11}^{(1)}W_1 + C_{33}c_{1N}^{(1)}W_N + C_{33}\sum_{k=2}^{N-1}c_{1k}^{(1)}W_k = 0 \\
&C_{55}c_{N1}^{(1)}U_1 + C_{55}c_{NN}^{(1)}U_N + C_{55}\beta_m W_N + C_{55}\sum_{k=2}^{N-1}c_{Nk}^{(1)}U_k = 0 \\
&C_{44}c_{N1}^{(1)}V_1 + C_{44}c_{NN}^{(1)}V_N + C_{44}p_n W_N + C_{44}\sum_{k=2}^{N-1}c_{Nk}^{(1)}V_k = 0 \\
&-C_{13}\beta_m U_N - C_{23}p_n V_N + C_{33}c_{N1}^{(1)}W_1 + C_{33}c_{NN}^{(1)}W_N + C_{33}\sum_{k=2}^{N-1}c_{Nk}^{(1)}W_k = 0
\end{aligned} \tag{18}$$

In order to carry out the eigenvalue analysis, domain and boundary degrees of freedom are separated and in vector forms they are denoted as (d) and (b), respectively. Based on this definition, the matrix form of the equilibrium equations and the related boundary conditions take the following form:

$$\begin{bmatrix}[A_{bb}] & [A_{bd}]\\ [A_{db}] & [A_{dd}]\end{bmatrix}\begin{Bmatrix}\{U_b\}\\ \{U_d\}\end{Bmatrix} = \begin{Bmatrix}\{0\}\\ -\omega^2[M]\{U_d\}\end{Bmatrix} \tag{19}$$

where $\{U_d\}$ and $\{U_b\}$ are as follows:

$$\{U_d\} = \{\{U_d\},\{V_d\},\{W_d\}\}^T \tag{20}$$

$$\{U_b\} = \{\{U_b\},\{V_b\},\{W_b\}\}^T \tag{21}$$

Eliminating the boundary degrees of freedom, this equation become:

$$\left([A] + \omega^2 [M]\right)\{U_d\} = \{0\} \tag{22}$$

where

$$[A] = [A_{dd}] - [A_{db}][A_{bb}]^{-1}[A_{bd}] \tag{23}$$

The above eigenvalue system of equations can be solved to find the natural frequencies of the FGS plate.

3 NUMERICAL AND RESULTS

To verify the proficiency of presented method and four-parameter model for volume fraction of FGM materials, two numerical examples are carried out for comparisons. As a first example, the convergence and accuracy of the method is investigated in evaluating the first four natural frequency parameters of the FG moderately thick plates. The results are prepared for different values of the DQ grid points in Table 1. As noticed, fast rate of convergence of the GDQ method is evident and it is founded that only 13 DQ grid in the thickness direction can yield accurate results for a graded plate. Also, one can see that excellent agreement exist between the results of this method and those of 2D higher order theory of Matsunaga [7].

For further verification of the results of new four-parameter model, by setting *a=1*and *b=0* in relation (2), the non-dimensional fundamental frequencies for the simply supported square sandwich plate with classic functionally graded faces and homogeneous core are listed in Table 2. The Young's modulus profile in this case is as shown in Fig 2a. It is seen that the present results agree well with those obtained through three-dimensional Ritz solution by Li et al. [8] as well as meshless global collocation method by Xiang et al. [15].

In this section, we characterize the response of FGS rectangular plate. The non-dimensional natural frequency is defined by $\Omega = \omega h\sqrt{\rho_c / E_c}$.

Table 1
Convergence behavior and accuracy of the first four non-dimensional natural frequencies ($\Omega = \omega h\sqrt{\rho_c / E_c}$) of a simply supported FG plate against the number of DQ grid points (*h/L1 =0.5*)

		p			Mode (n,m)
		(1,0)	(1,1)	(2,0)	(1,2)
4	N=9	0.3957663	0.59935	0.958488	1.103291
	N=13	0.357754	0.599487	0.958751	1.103656
	N=20	0.357758	0.599494	0.958764	1.103674
	[5]	0.3577	0.5995	0.9587	1.1037
	[7]	0.3579	0.5997	0.9591	1.1040
10	N=9	0.328012	0.541517	0.852797	0.978336
	N=13	0.331127	0.545802	0.858398	0.984311
	N=20	0.331146	0.545833	0.858445	0.984365
	[5]	0.3311	0.5458	0.8584	0.9843
	[7]	0.3313	0.546	0.8588	0.9847

Table 2

Comparison of none dimensional fundamental frequency ($\omega^* = \omega(\frac{L_1^2}{h})\sqrt{\rho_0 / E_0}$) for the simply supported square sandwich plates with classic FGM faces $(a=1, b=0, h/L_1=0.1, \rho_0=1kg/m^3, E_0=1GPa)$

p		h_f/h	
		1/3	4/10
1	Li et al. [8]	1.63053	1.67437
	Xiang et al. [15]	1.66476	1.70605
	Present	1.6778	1.7221
5	Li et al. [8]	1.78956	1.82611
	Xiang et al. [15]	1.84690	1.86177
	Present	1.7895	1.8371

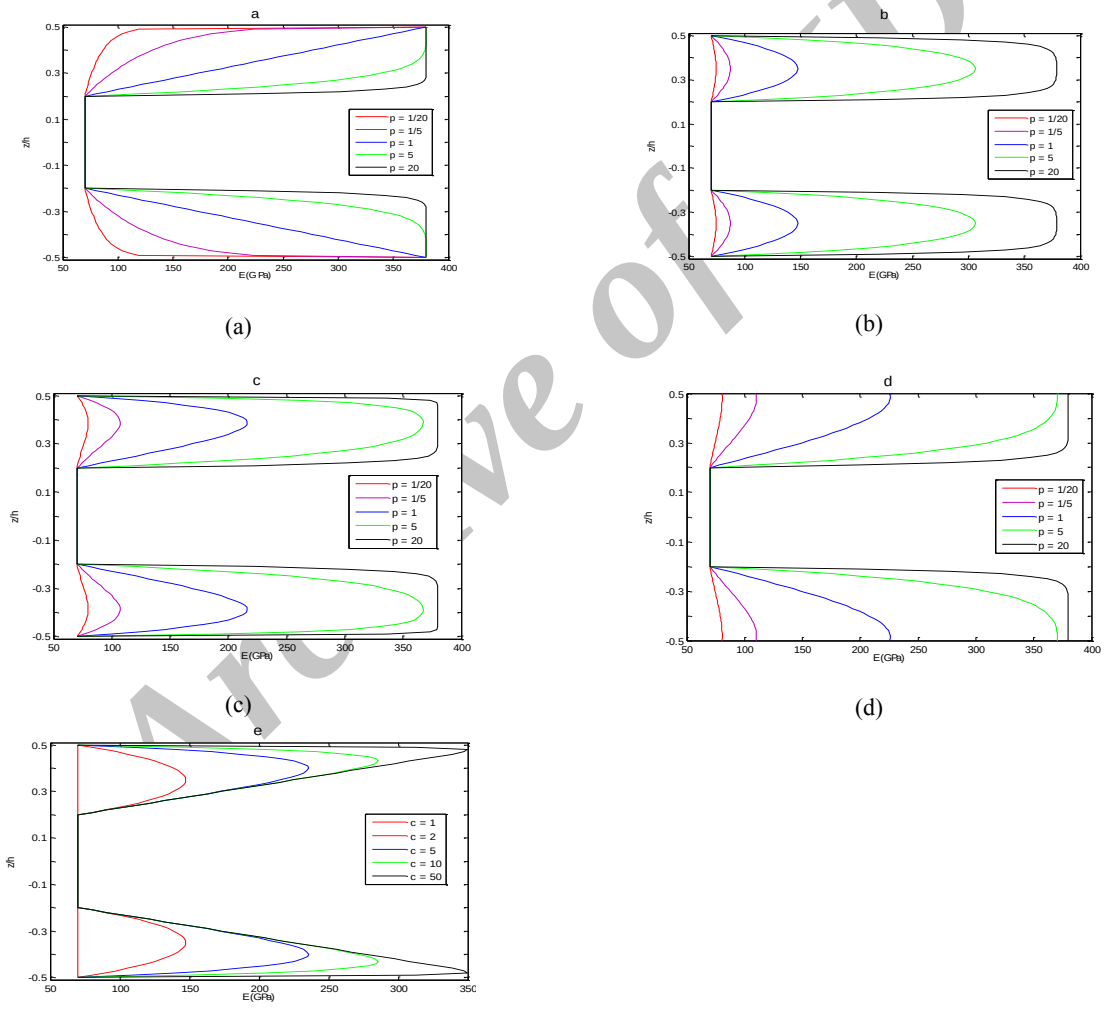

(a) (b) (c) (d) (e)

Fig. 2

Variation of the Young's modulus through the thickness in the FGS plate a: $a=1, b=0$, b: $a=1, b=1, c=2$ c: $a=1, b=1, c=4$, d: $a=0.8, b=0.2, c=2$, e: $a=0.8, b=0.3, p=3$.

The numerical results are tabulated in Table 3. for the symmetric FGS plates for the different values of p, geometrical parameter h/L_1 ratio and h_f/h ratio. The influence of the index p on the natural frequency of FGS plate is shown in Table 3. As can be seen from this table, increasing the value of the parameter index p up to infinity increases the contents of ceramic phase and at the same time reduces the percentage of metal phase in the sheets. In other words, relations 1 and 2 represent this fact that it is possible to obtain the homogeneous isotropic material in the sheets when the power-law exponent is set equal to zero or equal to infinity. Considering Table 3. , it is found that with increasing the value of p, the natural frequency, first, increases and then decreases. Also, the normalized natural frequency of FGS plate increases with increasing the h/L_1 ratio and h_f/h ratio for the different values of parameters p.

Table 3
First normalized natural frequency of the symmetric FGS plate for different values of power- law index p, h_f/h ratio and h/L_1 ratio ($L_1/L_2=1,\ a=1, b=1, c=2,\ n=1, m=1$)

h/L_1	h_f/h	p						
		0	1	2	5	10	50	∞
0.3	0.1	0.2173	0.2398	0.2527	0.2692	0.2740	0.2507	0.2362
	0.2	0.2173	0.2515	0.2698	0.2938	0.3054	0.2940	0.2602
	0.4	0.2173	0.2639	0.2893	0.3252	0.3475	0.3716	0.3411
0.4	0.1	0.3434	0.3741	0.3910	0.4122	0.4193	0.3925	0.3735
	0.2	0.3434	0.3893	0.4127	0.4426	0.4585	0.4532	0.4114
	0.4	0.3434	0.4114	0.4473	0.4978	0.5306	0.5749	0.5388
0.5	0.1	0.4780	0.5151	0.5349	0.5597	0.5689	0.5420	0.5200
	0.2	0.4780	0.5332	0.5602	0.5946	0.6147	0.6186	0.5723
	0.4	0.4780	0.5671	0.6133	0.6788	0.7228	0.7886	0.7490

The influence of the index p on the natural frequency is also shown in Figs. 3-5. The new and interesting result is that although it is expected the value of natural frequency parameter to be between the natural frequency parameter of the limit cases of homogeneous sheets of metal $(p=0)$ and of ceramic $(p=\infty)$, natural frequency parameter sometimes exceed the limit cases. It means though frequency parameter of the plate with ceramic rich sheets $(p=\infty)$ is more than the plate with metal rich sheets $(p=0)$, the frequency parameter of the sandwich plate doesn't necessarily increases with the increase of ceramic volume fraction. Since density of ceramic is more than metal, it means by choosing suitable values of *a, b, c* and *p*, frequency parameter can be obtained more than the frequency parameter of the similar FGS plate with sheets made of 100% ceramic and at the same time lighter. This result is because of using the four-parameter power-law distribution for FG materials. To explain the physically reason of this fact, as a very simple example, consider two mass-spring systems (systems 1 and 2) with single degree of freedom shown in Fig. 6. Results show that: $k_2 \succ k_1, M_2 \succ M_1, \omega_2 \succ \omega_1$.

Now, consider system 3. As observed $k_3 \prec k_2$ and $M_3 \succ M_2$ but $\omega_3 \succ \omega_2$. So, we can have a system with larger frequency, lower stiffness parameter and at the same time lighter than system 2. In other words, increasing the stiffness parameter does not necessary increase the frequency parameter.

Tornabene and Viola [1] came to the similar conclusion for four-parameter functionally graded conical, cylindrical shell and annular plate structures. Also, Yas et al. [20, 21] have obtained similar results for three-parameter FGM Euler-Bernolli beams.

Table 4. shows the influence of the parameter *c* on the first normalized frequencies for different values of h/L_1 and h_f/h ratio. In this Table, the Young's modulus profile of faces through thickness becomes asymmetric with increasing parameter *c* (as observed in Fig. 2e). As parameter *c* increases, the material's profile becomes asymmetric and then the frequency parameter increases for different values of h_f/h and h/L_1 ratio. The first normalized frequencies of different types of FGS plates are compared with each other in Table 5. for different values of h/L_1 ratio and h_f/h ratio. In this table, the Young's modulus profiles through thickness are classical for *a=1, b=0*, symmetric for *a=1, b=1*, *c=2* and asymmetric for *a=1, b=1*, *c=4*. It can be concluded from Table 5. that the normalized frequencies of symmetric profile are smaller than that of other types of FGS plates for different values of *p*, h_f/h ratio and h/L_1 ratio.

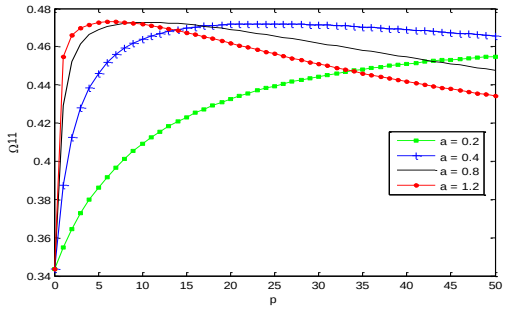

Fig. 3
Variation of the first non-dimensional natural frequency of FGS plate vs. the power-law exponent p for various values of the parameter a $(0.2 \le a \le 1.2,\ b=0.2,\ c=2,\ h/L_1=0.4,\ h_f/h=0.2)$.

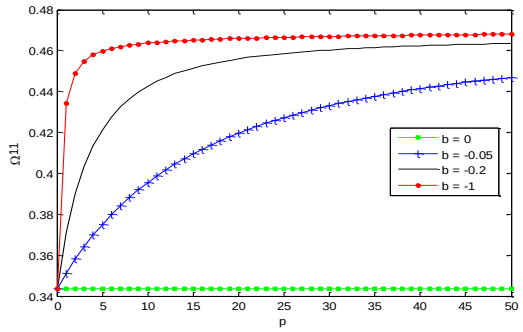

Fig. 4
Variation of the first non-dimensional natural frequency of FGS plate vs. the power-law exponent p for various values of the parameter b $(a=0,\ -1 \le b \le 0,\ c=2,\ h/L_1=0.4,\ h_f/h=0.2)$.

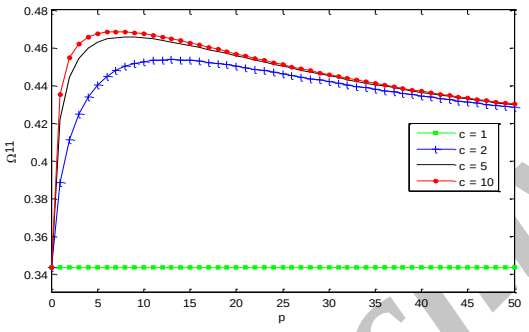

Fig. 5
Variation of the first non-dimensional natural frequency of FGS plate vs. the power-law exponent p for various values of the parameter c $(a=1,\ b=1,\ 1 \le c \le 10,\ h/L_1=0.4,\ h_f/h=0.2)$.

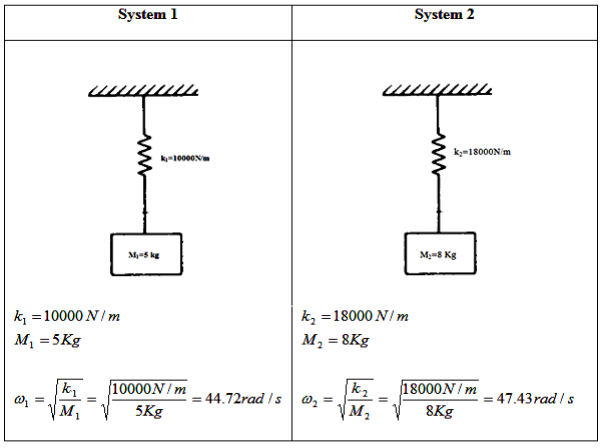

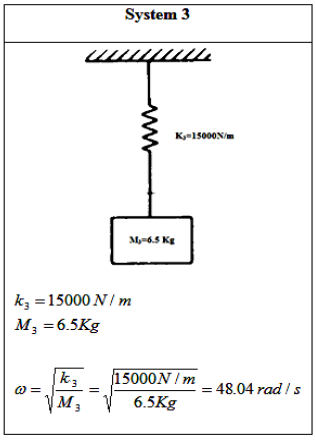

Fig. 6
Three simple mass-spring systems with single degree of freedom.

Also, it can be found, the normalized frequencies of classic profile are larger than that of other types of FGS plates for different values of p, h_f/h ratio and h/L_1 ratio. This fact that frequencies of symmetric and classic profiles are smaller and larger than that of other types of FGS plates respectively is also shown in Fig. 7.

The effect of length to width ratio of the FGS plate on the first non-dimensional natural frequency is shown in Fig.8. It results the non-dimensional natural frequency decreases with increasing the L_1/L_2 ratio and then remain almost unaltered for L_1/L_2 greater than 5 for different types of FGS plate.

Table 4
Variations of the first normalized natural frequency of FGS plate vs. the parameter c for various values of h_f/h ratio and h/L_1. ($L_1/L_2=1$, $a=1, b=1, p=1$, $n=1$, $m=1$)

h/L_1	h_f/h	c						
		2	4	8	13	20	30	50
0.3	0.2	0.2515	0.2731	0.2859	0.2915	0.2949	0.2971	0.2989
	0.3	0.2587	0.2842	0.2999	0.3069	0.3112	0.3140	0.3164
	0.4	0.2639	0.2942	0.3134	0.3223	0.3278	0.3315	0.3346
0.5	0.2	0.5332	0.5640	0.5819	0.5897	0.5945	0.5977	0.6003
	0.3	0.5480	0.5859	0.6085	0.6188	0.6253	0.6297	0.6334
	0.4	0.5671	0.6165	0.6460	0.6596	0.6683	0.6741	0.6792

Table 5
Comparison of fundamental normalized frequencies of different types of FGS plates for different values of h_f/h ratio and h/L_1 ratio ($L_1/L_2=1$, $n=1, m=1$)

h/L_1	h_f/h	p						
		0	1	2	5	10	50	∞
0.2	0.2							
	Classic	0.1079	0.1604	0.1676	0.1710	0.1699	0.1513	0.1290
	Asymmetric	0.1079	0.1417	0.1544	0.1658	0.1677	0.1511	0.1290
	Symmetric	0.1079	0.1280	0.1395	0.1550	0.1619	0.1503	0.1290
	0.4							
	Classic	0.1079	0.1802	0.1885	0.1932	0.1945	0.1922	0.1692
	Asymmetric	0.1079	0.1515	0.1677	0.1839	0.1902	0.1915	0.1692
	Symmetric	0.1079	0.1333	0.1477	0.1686	0.1810	0.1897	0.1692
0.5	0.2							
	Classic	0.4780	0.6044	0.6170	0.6262	0.6319	0.6217	0.5723
	Asymmetric	0.4780	0.5640	0.5900	0.6147	0.6266	0.6209	0.5723
	Symmetric	0.4780	0.5332	0.5602	0.5946	0.6147	0.6186	0.5723
	0.4							
	Classic	0.4780	0.6874	0.7170	0.7445	0.7617	0.7966	0.7490
	Asymmetric	0.4780	0.6165	0.6647	0.7184	0.7484	0.7944	0.7490
	Symmetric	0.4780	0.5671	0.6133	0.6788	0.7228	0.7886	0.7490

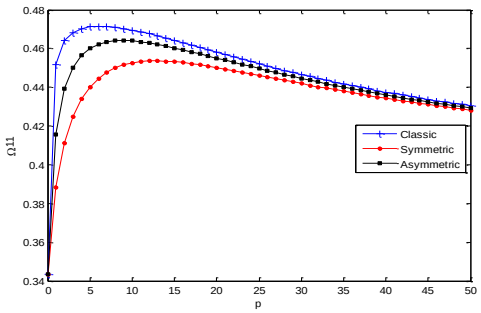

Fig. 7
Comparison of fundamental normalized frequencies of different types of FGS square plates ($h/L_1=0.4$, $h_f/h=0.2$).

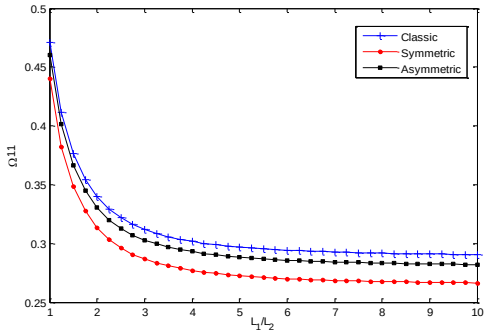

Fig. 8
The effect of length to width ratio of the FGS plate (L_1/L_2) on the non-dimensional natural frequency ($p=5$, $h/L_1=0.4$, $h_f/h=0.2$).

4 CONCLUSION

The GDQ method has been used to study three-dimensional free vibration analysis of functionally graded sandwich rectangular plate. The fast rate of convergence and accuracy of the method were investigated through the different solved examples. The two-constituent functionally graded plate consists of ceramic and metal which are graded through the thickness according to a four-parameter power-law distribution. From this study, some conclusions can be made:

Interesting result shows, by using the four-parameter power-law distribution and choosing suitable values of *a, b, c* and *p*, frequency parameter can be obtained more than the frequency parameter of the similar FGS plate with sheets made of 100% ceramic and at the same time lighter. This result is against the expected one for the frequency parameter of FGS plate to fall between those for p=0 (100% metal sheet) and p=∞ (100% ceramic sheet). Results show that normalized frequencies of symmetric and classic profiles are smaller and larger than that of other types of FGS plates respectively for different values of *p*, h_f/h ratio and h/L_1 ratio. It can be found, the normalized natural frequencies of FGS plate increase with increasing h_f/h ratio and h/L_1 ratio. As parameter *c* increases, the material's profile becomes asymmetric and then the frequency parameter increases for different values of h_f/h and h/L_1 ratio. It results the non-dimensional natural frequency decreases with increasing the L_1/L_2 ratio and then remain almost unaltered for L_1/L_2 greater than 5 for different types of FGS plates.

APPENDIX

$$L_{1x}=c_{11}\frac{\partial^2}{\partial x^2}+\frac{\partial c_{11}}{\partial x}\frac{\partial}{\partial x}+c_{66}\frac{\partial^2}{\partial y^2}+\frac{\partial c_{66}}{\partial y}\frac{\partial}{\partial y}+c_{55}\frac{\partial^2}{\partial z^2}+\frac{\partial c_{55}}{\partial z}\frac{\partial}{\partial z}$$

$$L_{1y}=c_{12}\frac{\partial^2}{\partial x\partial y}+\frac{\partial c_{12}}{\partial x}\frac{\partial}{\partial y}+c_{66}\frac{\partial^2}{\partial x\partial y}+\frac{\partial c_{66}}{\partial y}\frac{\partial}{\partial x}$$

$$L_{1z}=c_{13}\frac{\partial^2}{\partial x\partial z}+\frac{\partial c_{13}}{\partial x}\frac{\partial}{\partial z}+c_{55}\frac{\partial^2}{\partial x\partial z}+\frac{\partial c_{55}}{\partial z}\frac{\partial}{\partial x}$$

$$L_{2x}=c_{66}\frac{\partial^2}{\partial x\partial y}+\frac{\partial c_{66}}{\partial x}\frac{\partial}{\partial y}+c_{12}\frac{\partial^2}{\partial x\partial y}+\frac{\partial c_{12}}{\partial y}\frac{\partial}{\partial x}$$

$$L_{2y}=c_{66}\frac{\partial^2}{\partial x^2}+\frac{\partial c_{66}}{\partial x}\frac{\partial}{\partial x}+c_{22}\frac{\partial^2}{\partial y^2}+\frac{\partial c_{22}}{\partial y}\frac{\partial}{\partial y}+c_{44}\frac{\partial^2}{\partial z^2}+\frac{\partial c_{44}}{\partial z}\frac{\partial}{\partial z}$$

$$L_{2z}=c_{44}\frac{\partial^2}{\partial y\partial z}+\frac{\partial c_{44}}{\partial z}\frac{\partial}{\partial y}+c_{23}\frac{\partial^2}{\partial z\partial y}+\frac{\partial c_{23}}{\partial y}\frac{\partial}{\partial z}$$

$$L_{3x}=c_{55}\frac{\partial^2}{\partial x\partial z}+\frac{\partial c_{55}}{\partial z}\frac{\partial}{\partial x}+c_{13}\frac{\partial^2}{\partial z\partial x}+\frac{\partial c_{13}}{\partial x}\frac{\partial}{\partial z}$$

$$L_{3y} = c_{44}\frac{\partial^2}{\partial y \partial z} + \frac{\partial c_{44}}{\partial y}\frac{\partial}{\partial z} + c_{23}\frac{\partial^2}{\partial y \partial z} + \frac{\partial c_{23}}{\partial z}\frac{\partial}{\partial y}$$
$$L_{3z} = c_{11}\frac{\partial^2}{\partial x^2} + \frac{\partial c_{11}}{\partial x}\frac{\partial}{\partial x} + c_{66}\frac{\partial^2}{\partial y^2} + \frac{\partial c_{66}}{\partial y}\frac{\partial}{\partial y} + c_{55}\frac{\partial^2}{\partial z^2} + \frac{\partial c_{55}}{\partial z}\frac{\partial}{\partial z} \quad \text{(A.1)}$$

REFERENCES

[1] Tornabene F., Viola E., 2009, Free vibration analysis of four-parameter functionally graded parabolic panels and shells of revolution, *European Journal of Mechanics - A/Solids* **28**:991-1013.

[2] Sobhani B., Yas M.H., 2010, Three-dimensional analysis of thermal stresses in four-parameter continuous grading fiber reinforced cylindrical panels, *International Journal of Mechanical Sciences* **52**:1047-1063.

[3] Sobhani B., Yas M.H., 2010, Static and free vibration analyses of continuously graded fiber-reinforced cylindrical shells using generalized power-law distribution, *Acta Mechanica* **215**:155-173.

[4] Pourasghar A., Yas M.H., Kamarian S., 2013, Local aggregation effect of CNT on the vibrational behavior of four-parameter continuous grading nanotube reinforced cylindrical panels, *Polymer Composites* **34**(5):707-721.

[5] Malekzadeh P., 2008, Three-dimensional free vibrations analysis of thick functionally graded plates on elastic foundations, *Composite Structures* **89**(3):367-373.

[6] Yas M.H., Sobhani B., 2010, Free vibration analysis of continuous grading fiber reinforced plates on elastic foundation, *International Journal of Engineering Science* **48**:1881-1895.

[7] Matsunaga H., 2008, Free vibration and stability of functionally graded plates according to a 2D higher-order deformation theory, *Composite Structures* **82**:499-512.

[8] Li Q, Iu VP, Kou KP, 2008, Three-dimensional vibration analysis of functionally graded material sandwich plates, *The Journal of Sound and Vibration* **311**(1–2):498–515.

[9] Zenkour AM., 2005, A comprehensive analysis of functionally graded sandwich plates: Part1- deflection and stresses. *International Journal of Solids and Structures* **42**:5224–5242.

[10] Zenkour AM., 2005, A comprehensive analysis of functionally graded sandwich plates: Part2- buckling and free vibration deflection and stresses, *International Journal of Solids and Structures* **42**:5243–5258.

[11] Khalili S.M.R., Mohammadi Y., 2012, Free vibration analysis of sandwich plates with functionally graded face sheets and temperature dependent material properties: A new approach, *European Journal of Mechanics - A/Solids* **35**:61–74.

[12] Natarajan S., Manickam G., 2012, Bending and vibration of functionally graded material sandwich plates using an accurate theory, *Finite Elements in Analysis and Design* **57**:32–42.

[13] Neves A.M.A., Ferreira A.J.M., Carrera E., Cinefra M., Roque C.M.C., Jorge R.M.N., Soares C.M.M., 2013, Static free vibration and buckling analysis of isotropic and sandwich functionally graded plates using a quasi-3D higher-order shear deformation theory and a meshless technique, *Composites Part B: Engineering* **44**(1):657–674.

[14] Sobhy M., 2012, Buckling and free vibration of exponentially graded sandwich plates resting on elastic foundations under various boundary conditions, *Composite Structures* **99**:76-87.

[15] Song X., Gui-wen K., Ming-sui Y., Yan Z., 2013, Natural frequencies of sandwich plate with functionally graded face and homogeneous core, *Composite Structures* **96**:226–231.

[16] Bellman R, Kashef B.G., Casti J., 1972, Differential Quadrature: a technique for a rapid solution of non linear partial differential equations, *Journal of Computational Physics* **10**:40–52.

[17] Shu C., 2000, *Differential Quadrature and Its Application in Engineering*, Berlin, Springer.

[18] Kamarian S., Yas M.H., Pourasghar A., 2012, Free Vibrations of Continuous Grading Fiber Orientation Beams on Variable Elastic Foundations, *Journal of Solid Mechanic* **4**(1): 75-83.

[19] Bert CW., Malik M., 1996, Differential quadrature method in computational mechanics, a review, *Applied Mechanics Reviews* **49**:1-28.

[20] Yas M. H., Kamarian S., Eskandari J., Pourasghar A., 2011, Optimization of functionally graded beams resting on elastic foundations, *Journal of Solid Mechanic* **3**(4):365-378.

[21] Yas M.H., Kamarian S., Pourasghar A.,2012, Application of imperialist competitive algorithm a and neural networks to optimize the volume fraction of three-parameter functionally graded beams, *Journal of Experimental & Theoretical Artificial Intelligence* , doi:10.1080/0952813X.2013.782346.